Using a Multiscale Modeling Approach to Correlate Reaction Conditions with Polymer Microstructure and Rheology

Kristina M. Zentel,* Jonas Degenkolb, and Markus Busch*

Reaction conditions have a huge impact on the resulting polymer properties, but capturing this requires understanding the correlation of the underlying kinetics, the polymer architecture, and polymer flow behavior. Long-chain branched polymers created randomly by free-radical polymerization, such as low-density polyethylene (LDPE), show complex rheological behavior and are thus interesting in this context. A study applying a multiscale modeling approach is used to simulate varying reaction conditions and predict the structure of the resulting LDPE polymer and its flow properties. A significant effect on the molecular weight distribution, but also the viscosity and extensional flow behavior can be predicted. Higher conversions, for example, lead to broader molecular weight distributions, increased long-chain branching degrees, and a higher branching complexity. Consequently, also higher viscosities and increased strain hardening are observed in extension. Additionally, miniplant experiments are performed to resemble the simulations and compare the results. The accordance of predictions and analytical results are very good and validate the model over a wide range of reaction conditions.

1. Introduction

A consequent combination of experiments and modeling results is one of the most powerful techniques when it comes to efficient and effective answering of complex scientific issues. A challenge where this approach can be used effectively are the complex reaction networks of (free) radical polymerizations.

A macroradical can easily undergo numerous reaction paths, so that multidimensional distributions of macromolecular species are created—with molecular weight (MW), branching, and comonomer distribution being the most important parameters. This is the reason for the incredibly broad spectrum of polymer properties that can be tuned by adjusting a polymeric microstructure on a molecular level. As "polymers are products by process," their microstructure is—to a certain extent—directly controllable via process conditions.[1] This opens up a huge potential of process optimizations as well as aimed product designs for systems with interesting polymeric microstructures that are industrially relevant and fairly well understood.

One of those processes is the high-pressure free-radical polymerization of ethylene to low-density polyethylene (LDPE) under supercritical conditions. It is a remarkable example not only because of its high industrial relevance, but mainly because of its complex random branching distribution. The short- and especially long-chain branches (LCBs) impact material properties drastically.[2,3] The LCBs are introduced by an intermolecular transfer reaction of a propagation macroradical to a polymer molecule. The resulting mid-chain radical can then either undergo a β-scission reaction or propagate further by monomer addition, which forms LCBs. This is shown schematically in **Figure 1**. Full kinetic schemes of the LDPE polymerization can be found in the literature.[4,5]

LCBs are essential when it comes to polymer properties and processing behavior. They lead to effective size reduction of the polymer coil, which can be seen both analytically in light-scattering experiments[6] as well as by studying flow behavior. Rheological experiments show reduced viscosities for LDPE compared to linear high-density polyethylenes.[3,7] However, when the technically relevant strongly nonlinear flows in extension are investigated, LCBs lead to an increased network connectivity in the polymer melt and consequently reduce the rate of disentanglement, if an external force is applied. Thus, a pronounced increase of elongational viscosity with time is observed in extensional flows, which is referred to as strain hardening behavior and very beneficial in terms of processing operations such as blow molding, film blowing, foaming, or fiber spinning.[8]

Following this argumentation, understanding structure-property relationships and how they can be manipulated by choosing appropriate reaction conditions is extremely beneficial in the LDPE context. A three-step multi-scale modeling strategy was recently introduced by Pflug and Busch,[4] which demonstrates
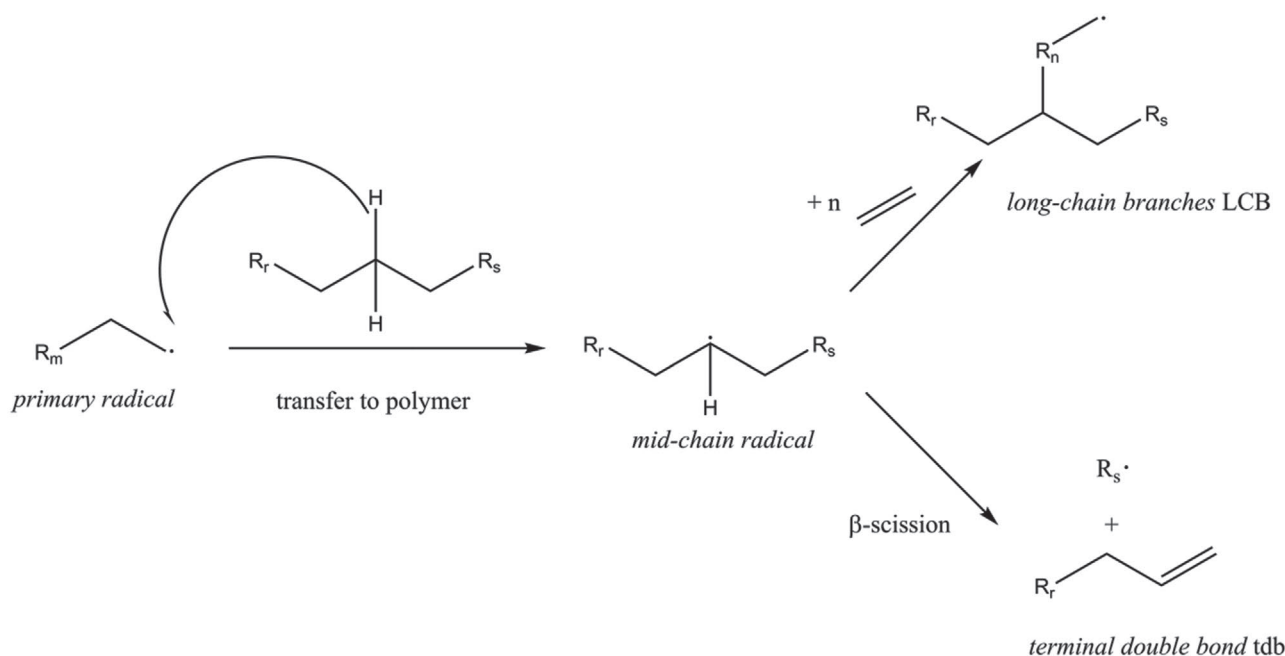
Dr. K. M. Zentel (formerly Pflug)
Institute for Technical and Macromolecular Chemistry
University of Hamburg
Bundesstr. 45, 20146 Hamburg, Germany
E-mail: kristina.zentel@chemie.uni-hamburg.de
J. Degenkolb, Prof. M. Busch
Institute for Technical and Macromolecular Chemistry
Technical University of Darmstadt
Alarich-Weiß-Straße 8, 64287 Darmstadt, Germany
E-mail: markus.busch@pre.tu-darmstadt.de

ADVANCED
SCIENCE NEWS
www.advancedsciencenews.com

Macromolecular
Theory and Simulations
www.mts-journal.de

Figure 1. Schematic depiction of long-chain branch (LCB) formation during free-radical polymerization of ethylene: transfer of a radical functionality from a propagation polymer to a dead polymer chain results in the formation of a mid-chain radical. It can either add monomer and form an LCB or undergo a β-scission reaction.

that the bridge from reaction conditions to polymer architectures and finally bulk properties in flow can be consistently build. Thereby the simulation starts with 1) the chemical process to synthesize the polymers (polymerization steps and all side reactions, scale: nm range), goes on to 2) the formation of a library of all possible (branched) polymers (Monte Carlo, scale: 100 nm) and ends 3) by putting the polyethylene (PE)-structures into a rheology model (branch-on-branch (BoB) algorithm, linear and nonlinear rheology, scale: mm range). This work is the ideal basis to further deepen and consolidate the effects of varying LDPE reaction conditions on branching density and type.

Therefore, the modeling strategy will be used to study the effect of different chemical surroundings on the resulting random branching structure. For this purpose, simulations with different chain-transfer agent (CTA) concentrations are modeled, as they determine the MW of the polymer chains. Moreover, different conversion regimes that resemble different polymer concentrations and thus different transfer probabilities are simulated.

In the next step, a very systematic set of high-pressure miniplant polymerization experiments are performed and subsequently characterized. This serves to check the previously made predictions and thus ensures model validity on a broad region of partially unusual reaction conditions. At the same time a deeper insight into the connection of microstructure and rheological properties of the complex randomly branched polyethylene samples can be gained. The beauty of combining experiment with simulations in this context is that only the model gives explicit branching structures of individual macromolecules, which are the basis of understanding how linear and nonlinear flow of BoB molecules works.

2. Experimental Section

2.1. Multiscale Modeling

A multiscale modeling approach can be used to directly connect reaction conditions with achievable polymer properties. The modeling strategy consists of three models that are directly interconnected with each other. A scheme of the work flow is shown in **Figure 2** and a short description of the modeling
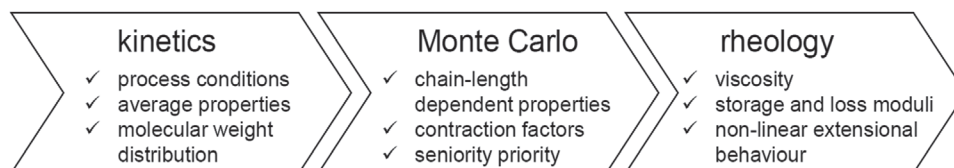
Figure 2. Three-step multiscale modeling strategy used within this work to connect reaction conditions with single macromolecular structures and finally bulk polymer processing properties. A deterministic model based on reaction kinetics and process conditions is linked via reaction probabilities to a hybrid stochastic Monte Carlo approach, which gives individual macromolecule topologies. Finally flow behavior of the calculated branched structures is modeled via a rheology model.

Table 1. Kinetic network and corresponding Arrhenius coefficients used for modeling the high-pressure ethylene polymerization: it consists of initiation, propagation, termination, and transfer reactions. I stands for the initiator, R_s for a radical of chain length s, P_s for a polymer of chain length s, E represents the monomer ethene and CTA the chain transfer agent. All reaction coefficients are denoted as $k_{reaction}$. In some cases mass-less counting species $H_{reaction}$ are introduced to monitor how often certain reaction are performed during the polymerization.

reaction	chemical equation	k_0 [L mol^{-1} s^{-1} or s^{-1}]	E_A [kJ mol^{-1}]	ΔV [cm^3 mol^{-1}]	Literature
Initiation	$I_2 + 2E \xrightarrow{k_{d,ini}} 2 f_{ini} R_1$	7.05×10^{15}	150.4	18.2	[16]
Propagation	$R_s + E \xrightarrow{k_p} R_{s+1}$	1.88×10^7	34.30	−27.0	[5]
Transfer to monomer	$R_s + E \xrightarrow{k_{trM}} P_s + R_1$	3.42×10^8	75.95	−5.6	[17]
Transfer to CTA	$R_s + CTA \xrightarrow{k_{trCTA}} P_s + R_1$	3.44×10^6	26.80	−14.9	[5]
Transfer to polymer	$R_s + P_r \xrightarrow{k_{trPM}} R_{r,MCR} + P_s$	1.02×10^8	49.15	−3.4	[18]
β-scission	$R_{s,MCR} \xrightarrow{k_\beta \cdot f(s,r)} R_{s-r} + P_r$	3.21×10^8	42.56	−30.8	[5]
Formation of LCB	$R_{s,MCR} + E \xrightarrow{k_p} R_{s+1} + H_{LCB}$	1.88×10^7	34.30	−27.0	[5]
Backbiting	$R_s \xrightarrow{k_{bb}} R_s + H_{SCB}$	1.60×10^8	45.78	−23.3	[5]
Disproportionation	$R_s + R_r \xrightarrow{k_{t,disp}} P_s + P_r$	8.11×10^8	46.00	15.8	[5]
Recombination	$R_s + R_r \xrightarrow{k_{t,comb}} P_{s+r}$				
Propagation of tDB	$R_s + P_r \xrightarrow{k_{tdb} \cdot f(r)} R_{s+r,MCR} + H_{tDB}$	6.00×10^7	34.30	15.8	[19]

approach is given in this section. For a description of the full modeling strategy, the reader is referred to the literature.[4]

The first step is a kinetic model, which numerically solves the system of differential equations of mass, enthalpy, and impulse balance. It is based on the reaction network of the free-radical polymerization of ethylene and includes the respective kinetic coefficients, all reagents, and their thermophysical properties and concentrations as well as reactor configuration. The kinetic network of the LDPE polymerization is given in **Table 1** together with the corresponding rate coefficients used for modeling. Termination is performed via combination and disproportionation, which are not equally likely. The coefficient in Table 1 gives the sum of them, while the ratio can be calculated according to **Table 2**. It also contains a correlation for the conversion dependence of viscosity and the viscosity effect on propagation and termination. The model is set up in the commercial software Predici[9] and gives concentration profiles of all species, conversion as well as average polymer properties. This includes number and weight, average MW, average long- and short-chain branching frequencies as well as the MW distribution. Moreover, reaction probabilities of the individual macromolecular species are derived from the kinetic model and used as input for the consecutive Monte Carlo simulation.

Those are then applied to model exact branching structures of individual macromolecules in the hybrid stochastic Monte Carlo algorithm based on drawing pseudo-random numbers. It is an individual macromolecule approach, which calculates topologies of an ensemble of macromolecules one after the other depending only on reaction conditions as implemented in the kinetic model.[10] A reaction frequency R_i is calculated for each reaction i of the network by the deterministic model. The reaction frequency is defined as the corresponding reaction rate divided by considered moment of the respective polymeric species. Then, the hybrid Monte Carlo approach uses the reaction frequencies to calculate event probabilities for the individual reactions P_i according to Equation (1).

$$P_i = \frac{R_i}{\sum R_i} \tag{1}$$

Table 2. Ratio of combination and termination,[20] viscosity as a function of conversion, and effect of viscosity on propagation and termination rate for the high-pressure polymerization of ethylene.[21]

Combination / termination	$\dfrac{k_{t,comb}}{k_{t,disp}} = 3.321 \cdot \exp\left(\dfrac{1248 - 0.903 \cdot p\,[\text{bar}]}{R \cdot T\,[\text{K}]}\right)$
Relative viscosity	$\log \eta_r = 5.39 \cdot X + 3.7 \cdot \sqrt{X}$
Propagation	$k_p = \left(\dfrac{k_p^0}{1 + \dfrac{k_p^0}{1.13 \cdot 10^{10}} \cdot \eta_r}\right)$
Termination	$k_t = \left(\dfrac{0.832}{\eta_r} + 8.04 \cdot 10^{-6} \cdot (1-X) \cdot k_P\right) \cdot k_t^0$

**ADVANCED
SCIENCE NEWS**
www.advancedsciencenews.com

**Macromolecular
Theory and Simulations**
www.mts-journal.de

By drawing a random number (rand), a reaction path can be chosen. In addition to the reactions, the residence time of the individual molecules has to be taken into account. In case of an ideal continuously stirred tank reactor (CSTR), which we are assuming here, each molecule can be assigned an individual residence time t by using the cumulative residence time distribution $F(t/\tau)$ according to Equation (2).

$$rand = F(t/\tau) = 1 - \exp(-t/\tau) \tag{2}$$

After each reaction step of a macromolecule, a time step Δt is performed based on the algorithm developed by Gillespie (Equation (3)) and as soon as the summed time steps for a molecule exceed its individual residence time t, the macromolecule is considered to leave the reactor and thus finished.

$$\Delta t = \frac{\ln(rand)}{\sum R_i} \tag{3}$$

Its individual topology is stored and the next molecule is modeled. If a representative set of macromolecules is finished, chain-length dependent features of the microstructure can be evaluated. In this case five million molecules proved to be a sufficient molecule set with respect to reproducible prediction polymer properties as well as rheology. Calculations with higher numbers show less scattering but a comparable convergence, so that five million were chosen with respect to computational efficiency. Within this work, the focus was on the LCBs per 1000 carbon atoms and the branching ratio g as a function of MW. The branching ratio is a measure of coil contraction of a long-chain branched macromolecule in comparison to a linear macromolecule with the same MW (Equation 4).

$$g = \frac{(R_{g,s,\text{branched}}^2)}{(R_{g,s,\text{linear}}^2)} \tag{4}$$

The calculation of radius of gyration for the stochastically produced branched macromolecules is performed with the application of a 3D random walk. It generates random conformations on the basis of the individual topologies and uses them to calculate $(R_{g,s,\text{branched}}^2)$.

Moreover, seniority and priority values of individual polymer segments (polymer strand between two branch points, one branch point, and a chain end or two chain ends) can be determined and compared between different samples.[11] These values are associated with rheological flow properties of long-chain branched polymers and can be applied to learn something about branching type and relaxation behavior of a sample. The seniority s of a segment can be calculated by determining the number of segments to the furthest chain end on each side of the segment. The lower of the two values will be the segments' seniority. Long-chain branched macromolecules relax hierarchically, meaning from the terminal segments inwards. Thus, seniority is a measure of the structural depth and the relaxation time of a segment. Terminal segments have a seniority of $s = 1$ and consequently relax first. In contrast, the priority p of a segment is determined by calculating the number of chain ends connected to each side of that segment. Again the lower
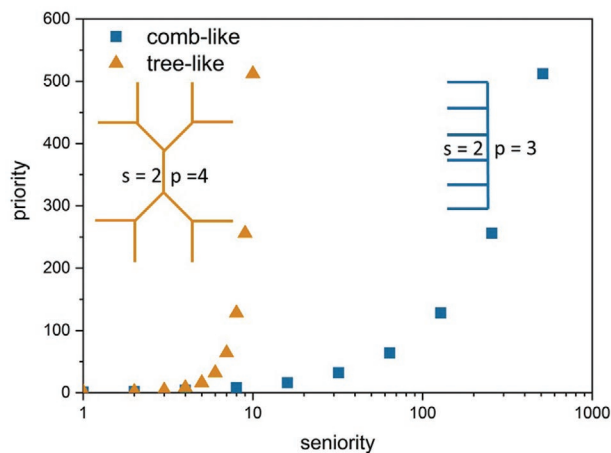
Figure 3. Seniority priority plots for an ideal comb polymer and an ideal Cayley tree. The central segment of the comb polymer has a seniority of $s = 2$ and a priority of $p = 3$, while the Cayley tree exhibits $s = 2$ while $p = 4$.

value is regarded as the priority, and terminal segments exhibit a priority of $p = 1$. Priority is associated with the maximum tension a segment can support in the context of nonlinear flows in extension. Thus, it is crucial when evaluating the anchoring behavior of branch points that finally lead to strain hardening on long-chain branched polymer materials. An exemplary seniority priority plot for an ideal comb and an ideal star polymer is given in **Figure 3**. Seniority and priority values were calculated for the innermost segment to highlight the difference for those two structural boundaries.

The third and final step of the modeling strategy is modeling flow properties via the BoB algorithm.[11] A representative set of branching structures calculated during Monte Carlo simulation is sampled and used as input for BoB. This algorithm can model rheological behavior of branched polymer systems in the linear and nonlinear flow regimes, if the branching structure is known precisely. It performs time steps on a logarithmic scale and models relaxation processes via reptation as well as arm retraction. For randomly branched LDPE this is crucial, because its viscoelastic properties depend on both MW as well as long-chain branching and they are key criteria for polymer processing.

2.2. Miniplant Experiments

The LDPE samples used within this work were produced in the high-pressure labs of Technische Universität Darmstadt. The high-pressure polymerization experiments are conducted in a high-pressure miniplant. The respective flow diagram is shown in **Figure 4**.

The centerpiece is a 100 mL autoclave, which can be operated up to pressures of 2500 bar and temperatures up to 300 °C. It is equipped with a stirrer, which is operated at a frequency of 15 Hz in order to obtain a thorough mixing. Temperature and pressure within the reactor are monitored with a thermocouple and a pressure transducer, respectively. All experiments are performed at 2000 bar and 250 °C. Molar mass of LDPE was varied by adjusting the CTA flow, while conversion is varied by
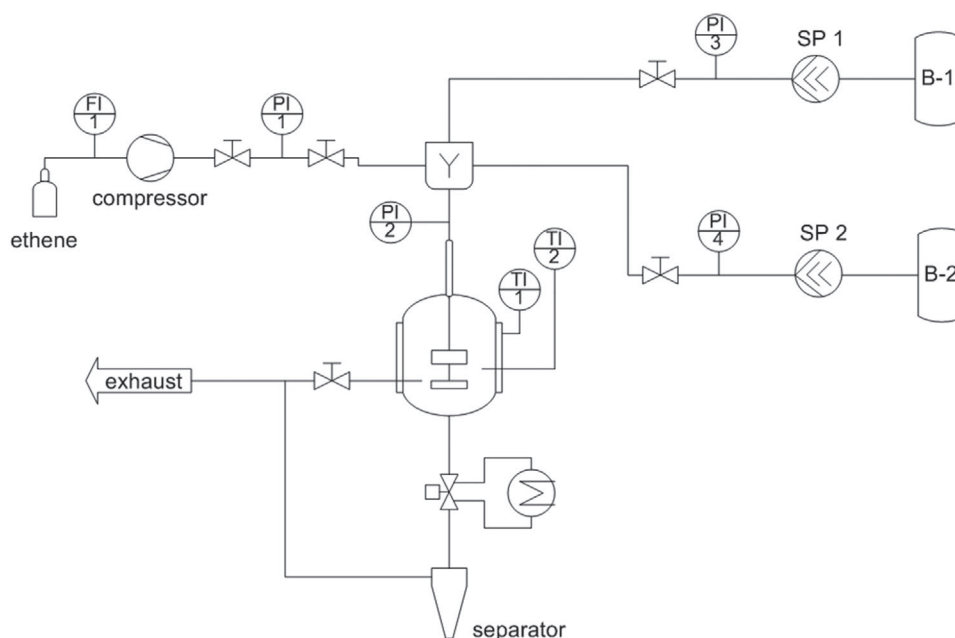
Figure 4. Flow chart of high-pressure polymerization mini plant. It consists of three feed streams: an ethene feed stream via a compressor and two syringe pumps (SP) for continuous liquid dosing. The stirred autoclave reactor is equipped with a heating jacket, two thermocouples, and a safety rupture disk. Reaction mixture is released into the separator/collecting vessel via a pneumatic valve.

simultaneously adjusting the initiator stream and the heat input by the jacket heating. Hereby, tert-butyl peroxyacetate dissolved in n-heptane is used as an initiator and pure propionic aldehyde (PA) is used as a CTA. Prior to any experiment, the reactor is cleaned, mounted in the high-pressure miniplant, and a pressure test is performed to secure the tightness of the system. After a successful pressure test, the autoclave is flushed with ethylene three times to remove residual oxygen and then pressure is released to 100–200 bars. The CSTR is heated to the desired reactor temperature (typically 220 °C). The mixtures of initiator and heptane as well as CTA are transferred into the respective storage tank of the two syringe pumps. Subsequently, both tanks are stripped with nitrogen for 15 min to remove residual oxygen. As soon as the desired reactor temperature is reached, the reactor is pressurized with a membrane compressor, and the proportional–integral–derivative controller of the pneumatic outlet valve maintains a steady pressure of 2000 bar at a set ethylene flow rate of 2 kg h^{-1}. The syringe pumps are compressed to 2000 bar, the desired initiator and CTA volume streams are set and polymerization is started. After the fivefold residence time and if steady temperature and pressure profiles are present, steady-state conditions are reached within the reactor. After additional 5 min the first sample is taken. Standard sampling time is 15 min. Only for the 1% conversion sample, sampling time was increased to 30 min in order to yield sufficient material. After a sample is taken, conditions are adjusted to meet the next desired process conditions. The next sample is taken only at the next steady state. Conversion is calculated by weighing the resulting sample while taking into account the ethylene volume stream.

Size exclusion chromatography (SEC) was performed using a high temperature PolymerChar GPC-infrared (IR) system (Polymer Char Laboratories Ltd.) equipped with an IR5 detector in hyphenation with a Wyatt Dawn Heleos II LS detector and an online Visco H502 viscometer detector, an Agilent 1200 autosampler, three Shodex UT 806M columns, one Shodex UT 807 column, and a Shodex UT-G guard column. The columns and detectors are operated at 150 °C. The eluent 1,2,4-trichlorobenzene (TCB) was distilled prior to its use and stabilized with 2,6-d-tert-butyl-4-methyl phenol (butylhydroxytoluene, 0.0125%). A flow rate of 1 mL min^{-1} was applied. All samples (2 mg) were dissolved in TCB (2 mL) for 1–2 h at 160 °C and 0.19 mL of the solutions were injected. Linear polystyrene standards (PSS Polymer Standards Service GmbH) with narrow MW distributions (MWD) were used for the IR calibration. Universal calibration was used to evaluate the visco detector data. The Mark–Houwink coefficients for linear PE were taken from the literature (K = 53 10^{-3} mL g^{-1} and α = 0.703).[12] A mixture of linear PE samples was used as a linear reference for the Mark–Houwink plot in the GPC One software (PSS, Dow and University of Konstanz). The MW dependent radii of gyration of linear PE, which are used as the reference when calculating branching ratios from multiangle laser light scattering (MALLS) data, were taken from Wang et al. $\left(\langle R_g^{1/2}\rangle = 2.86\ 10^{-2}\ M^{0.568}\right)$.[13] The MW distributions as well as the IR and visco data are evaluated using Polymer Char's GPC One software. The MALLS data were processed with the Astra software (Wyatt Technology, version 6.1.7.17) and a dn/dc value of −0.1040 mL g^{-1} was used for all samples.

Special care was taken to avoid changes in microstructure of the samples during rheology measurements. Prior to the rheological characterization, the samples were stabilized with 0.8 wt% Irganox 1010 and 0.8 wt% Irgafos 168 and hot-pressed at 200 °C and 200 bar into discs or strips of 1 mm thickness. Additionally, all experiments were performed under nitrogen

**ADVANCED
SCIENCE NEWS**
www.advancedsciencenews.com

**Macromolecular
Theory and Simulations**
www.mts-journal.de

atmosphere. Repetitive experiments were performed and gave identical results. The linear rheological response was measured on Physica MCR 300 Anton Paar rheometers or a TA Instruments ARES G2. Dynamic-mechanical measurements were performed using a 25 mm parallel plate geometry with a sample thickness of 1 mm in the linear range of deformation (5%). The frequency range was 0.02 s^{-1} to 628.3 s^{-1}. Elongational Rheology was measured using the optional stretching device SER. The sample strips were camped onto the counter-rotating cylinders and tempered prior to the testing. Hencky strain rates $\dot{\varepsilon}$ from 0.05 s^{-1} to 10 s^{-1} were applied.

3. Results and Discussion

This work is divided into two parts: In a first step a sensitivity study was performed by modeling with the aim to theoretically determine the impact of varying reaction conditions on resulting polymeric microstructure and processing properties. At the same time it should serve as an experimental design and a feasibility study for the next step. In order to test model sensitivity, preciseness, and boundaries, the simulated reaction conditions were used to prepare real LDPE samples in a second step. Obtained samples were analyzed and compared with expected modeling results.

The reactor setup investigated within this paper is a continuously operated miniplant autoclave reactor (details described in the Experimental Section). This is highly attractive from several points of view: In a miniplant setup, unusual and interesting reaction conditions can be realized much easier—or at all—compared to industrial plants. Only this makes the investigation of model boundaries and sensitivities possible. Additionally, the application of a single zone autoclave reactor—in contrast to industrially relevant multizone autoclave or tubular reactors—allows the application of very well-defined and controlled reaction conditions. This reduces the number of independently varying parameters that all affect microstructure and would be too complex to interpret especially from an experimental point of view.

3.1. Predicting Polymer Properties

A total number of 18 simulations were performed with the introduced three-step modeling approach. They were performed for identical temperatures and pressures, residence times, and ethene mass flows, while MW and conversion were systematically varied to investigate the impact of varying process conditions on polymeric microstructure. CTA feed was changed from 1 mL h^{-1} to 5 mL h^{-1} in order to prepare polymers with different average MW s. PA was chosen as CTA due to its high transfer constant. Consequently, only small amounts are necessary to access a broad MW area, which is desirable also from an experimental point of view. Moreover, conversion was chosen to vary from 1% to 13 %. This covers the experimentally accessible conversion range of the miniplant reactor and was achieved by adjusting initiator mass flow from a modeling point of view. For a bulk polymerization like the high-pressure polymerization of ethene a changing conversion directly corresponds to a modi-

Table 3. Summarized reaction conditions as used for the performed miniplant simulations. All simulations were performed at 250 °C, 2000 bar, a residence time of 90 s, and an ethene mass flow of 0.556 g s^{-1}. Initiator efficiency chosen based on previous modeling of tert-butyl peroxyacetate-initiated miniplant experiments at TU Darmstadt and TBPA mass flow was adjusted to meet desired conversion.

simulation	$\dot{V}_{CTA}$ [mL h^{-1}]	conversion [%]	$\dot{m}_{TBPA}$ [g s^{-1}]
1	1.0	1	4.4×10^{-8}
2	2.5	1	4.4×10^{-8}
3	5.0	1	4.4×10^{-8}
4	1.0	5	5.65×10^{-7}
5	2.5	5	5.65×10^{-7}
6	5.0	5	5.65×10^{-7}
7	1.0	7	9.85×10^{-7}
8	2.5	7	9.85×10^{-7}
9	5.0	7	9.85×10^{-7}
10	1.0	9	1.53×10^{-6}
11	2.5	9	1.53×10^{-6}
12	5.0	9	1.53×10^{-6}
13	1.0	11	2.20×10^{-6}
14	2.5	11	2.20×10^{-6}
15	5.0	11	2.20×10^{-6}
16	1.0	13	3.00×10^{-6}
17	2.5	13	3.00×10^{-6}
18	5.0	13	3.00×10^{-6}

fied polymer concentration. This is interesting in the context of long-chain branching and polymer processability. LCBs are formed during a transfer-to-polymer step (compare Figure 1) and thus their formation rate is directly proportional to the number of polymerized ethylene units. A detailed overview of chosen reaction conditions for the 18 simulations is found in **Table 3**.

The MWD as received from the deterministic (lines) and stochastic model (dots) are given in **Figure 5**. The overall agreement of deterministic and stochastic modeling results is good and serves as independent model validation. While on the left side MWDs for a conversion of 1 %, but systematically varying CTA feed are shown, the right side pertains to 13 % conversion. For both figures it can be easily seen that an increase of CTA feed results in a decrease of average MW (maxima of the MWDs are shifted to lower MW). This corresponds to expectations of increased transfer events, which result in shorter chains. At the same time, the broadness of the distributions increases both with decreasing CTA feed and with increasing conversion (from 1% to 13 %). This can be attributed to an increased transfer-to-polymer reaction with increasing polymer concentration, which is synonymous to increasing conversion. An increased transfer-to-polymer rate results in the creation of more high-MW material, which consequently also exhibits a more diverse branching behavior. Accordingly, MWDs are broadened and this effect is further enhanced for increasing average MWs. Deviations between the kinetic model and the deterministic model in the high-MW area for model polymers with high MW are caused
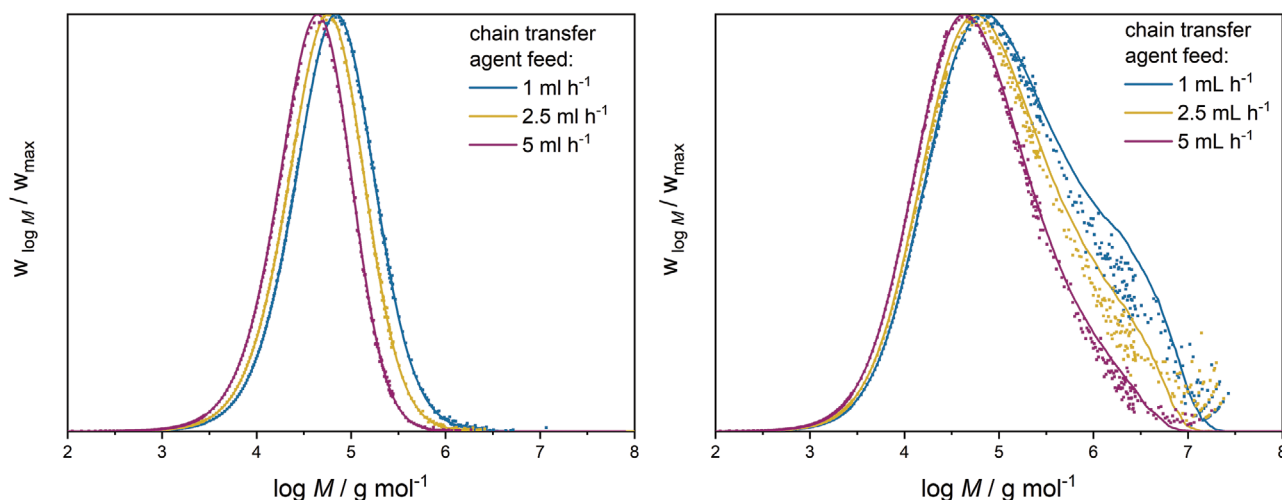
Figure 5. Deterministically (lines) and stochastically (dots) molecular weight distributions for a conversion of X = 1% (left; simulations 1, 2, and 3) and conversion of X = 13% (right; simulations 16, 17, and 18) but varying CTA feed streams.

by the assumption of nontopological scission within the kinetic model. In the kinetic model the simplifying assumption is made that the fragment length probability during β-scission is constant for all polymers, while it actually depends on branching structure for long-chain branched polymers.[14] This so-called "topological scission" is automatically accounted for correctly in the Monte Carlo algorithm, as individual macromolecules are considered for β-scission depending on their unique branching structures.

The individual branching structures produced by the hybrid Monte Carlo algorithm can then be used to evaluate the materials microstructure. Long-chain branching frequency in units of LCB/1000C can directly be extracted from the simulation results. The branching ratio as a function of MW is determined by a random walk and seniority and priority values are calculated according to their definition. The combined microstructural information for simulations 16, 17, and 18 (see Table 3) is given in **Figure 6**. This allows the direct assessment of the impact of average chain length on molecular structure. It can be seen that LCB frequency slightly increases with increasing CTA feed, which means reduced chain-length. This can be explained by the fact that a reduced chain-length at a constant conversion is synonymous to an increase of polymer concentration, so that the transfer to polymer reaction is more probable and more LCBs are formed. Consequently a decrease of branching ratio g is expected and also observed. However, it is not nearly as pronounced as expected. This is the first hint that chain contraction due to long-chain branching is not a very sensitive parameter above a certain branching degree. While seniority values are similar for the three simulations, priority values decrease significantly with increasing CTA feed stream. This demonstrates nicely that a reduced average MW results in a reduction of branching depth in terms of BoB structures and branching complexity. It might sound counterintuitive at first that an increased branching frequency for lower average MWs corresponds to a less complex branching structure and consequently reduced strain hardening behavior. But rheology is governed by the small fraction of highest MW, which is highly

branched in terms of branches per molecule and strongly increased for a higher average chain length.

The same microstructural characteristics are shown for simulations with the same average MW but systematically varying conversions from 1% to 13% (simulations 3, 6, 9, 12, 15, and 18) in **Figure 7**. One reason for modeling experiments with identical MW but at different conversions was that the effect of LCBs on rheological properties was of interest. The effect of increasing LCB frequency with increasing conversion is clearly visible in the first graph. However, the impact of the significantly increasing LCB frequency on branching ratio is small. Only simulation 3 for a conversion of 1%, which exhibits a strongly reduced LCB frequency, shows a significantly changed branching ratio. When taking into account the error and light-scattering data used to experimentally determine branching ratios, it will be very challenging up to impossible to distinguish them. Moreover, up till now the branching ratio was considered to be a sensitive measure to both branching frequency and branching type (star vs comb structure). However, the presented results indicate that the computationally determined branching ratio is primarily governed by branching structure and—above a certain degree of branching—rather insensitive regarding absolute frequency. In combination with the considerations, which were already drawn in the context of light-scattering analytics and model assumptions, the branching ratio g should not be overinterpreted when it comes to quantifying branching. This is an unexpected but valuable conclusion, which can be drawn from the presented sensitivity study.

The seniority priority plots for varying conversion exhibit increasing priorities with increasing conversion. This can be attributed to higher branching at higher conversion, which leads to more densely branched molecules and consequently higher priority values (higher number of chain ends on one side of the segment). From the rheological perspective this will result in a more pronounced strain hardening behavior.

The microstructural evaluation is followed by the evaluation of the respective flow behavior. The linear shear and nonlinear extensional rheology with a varying molar mass (simulations
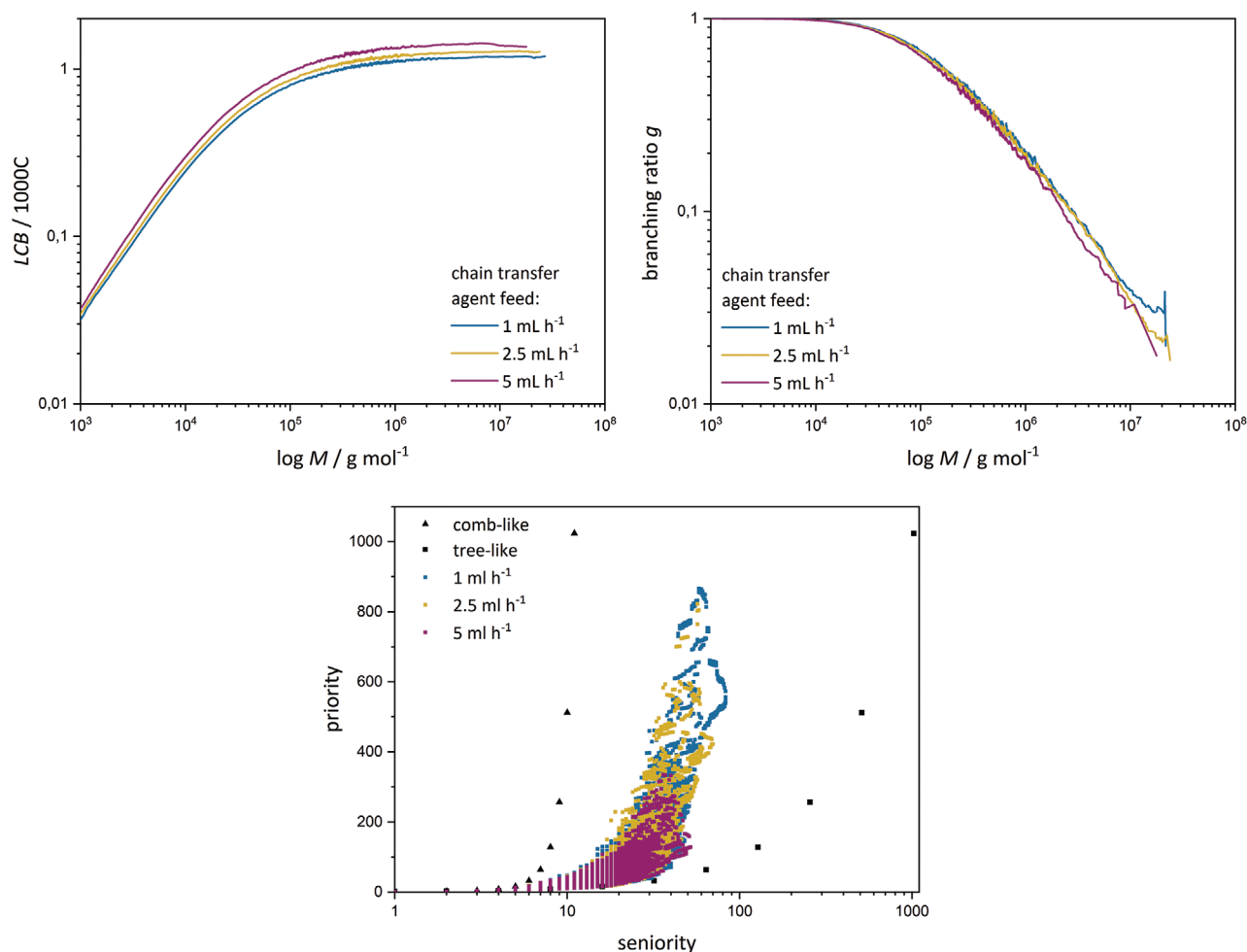
Figure 6. Microstructural properties of model polymers calculated for a conversion of 13% but for different CTA feed streams (16, 17, and 18), thus resembling samples with different average molecular weight.
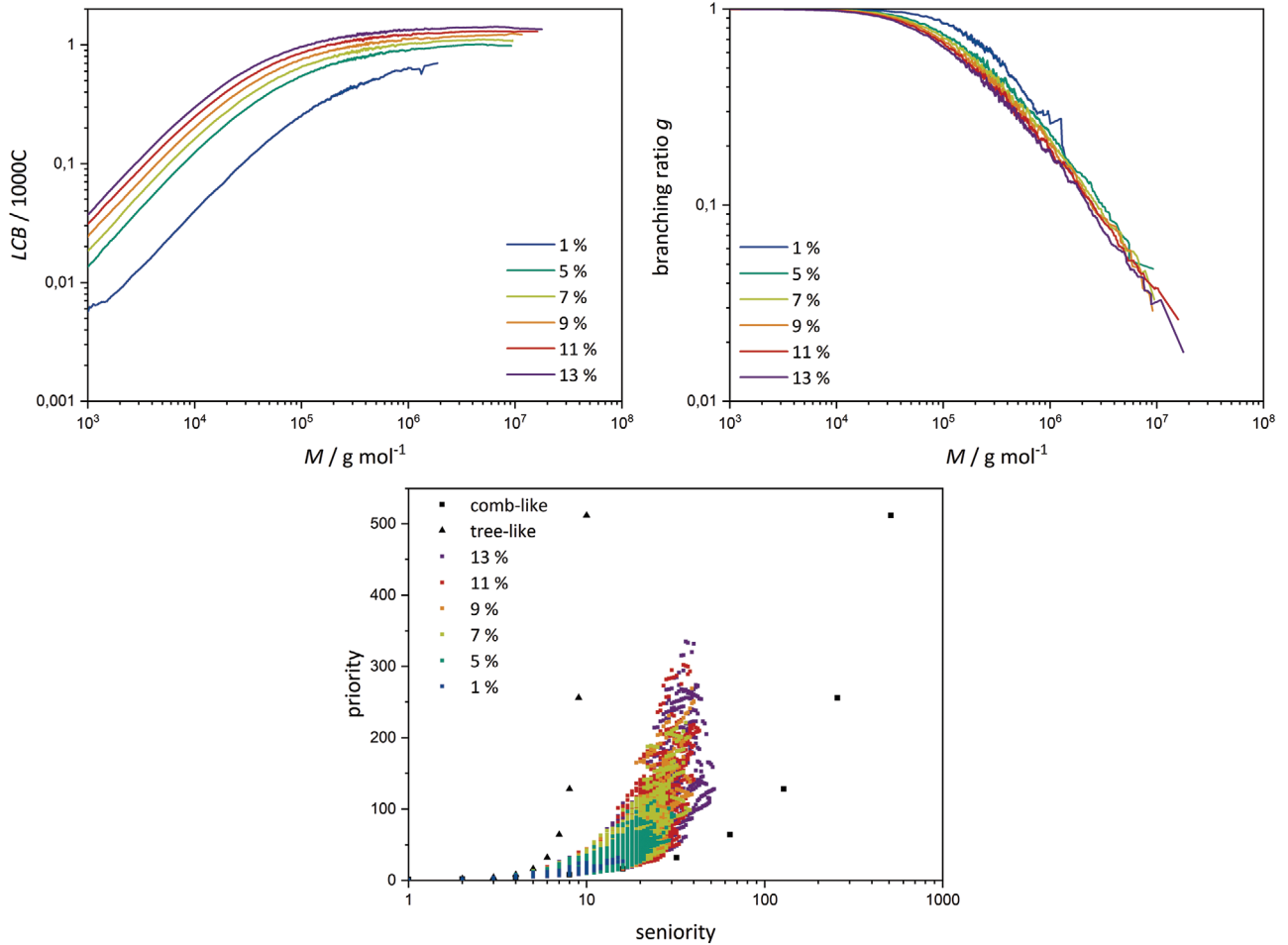
16, 17, and 18) is shown in **Figure 8**. Linear shear rheology is strongly affected by MW. With decreasing molar mass, storage and loss moduli are also decreasing, especially in the low-frequency range. The latter corresponds to the terminal relaxation regime, which is dominated by long chains. The intersections of storage and loss modulus, also referred to as cross-over points, are shifting to high frequencies with decreasing molar mass. This also agrees with the expectation that lower molar masses result in lower viscosities and a more pronounced elastic part. Extensional viscosities also exhibit very different characteristics with a varying molar mass. The absolute viscosity values differ in analogy to the linear viscoelasticity. The onset of strain hardening is similar for the three simulations, but as expected from the seniority priority plots an increased average MW results in stronger strain hardening.

In **Figure 9** the effect of varying LCB content but for constant average MW on rheology is depicted (simulations 3, 6, 9, 12, 15, and 18). Storage and loss moduli of those model polymers are identical within the experimental error of the technique with the exception of the 1% conversion simulation. This means that these samples are indistinguishable by linear shear rheology,

although they are clearly differing strongly regarding their polymeric microstructure and branching densities. This can be seen when investigating the respective extensional viscosities. Although the level of viscosity and onset of strain hardening are very similar for those materials, they exhibit strongly differing plateaus of strain hardening. As expected from the only qualitative seniority priority plots, strain hardening increases with increasing conversion and thus both branching content and depth.

The primary goal of the conducted sensitivity study was to demonstrate the strength of the developed three-step modeling strategy with respect to connecting reaction conditions with polymer properties. It could also give valuable insights into the sensitivity of various observables regarding MW and branching density. By this the sensitivity study demonstrated how modeling helps to identify, if a certain set of experiments is likely to be sensitive toward the desired experimental outcome in advance. Furthermore, it could clearly be presented, that this multidimensional and entangled system can only be tackled by a consequent combination of various modeling and characterization techniques. They can capture the complex
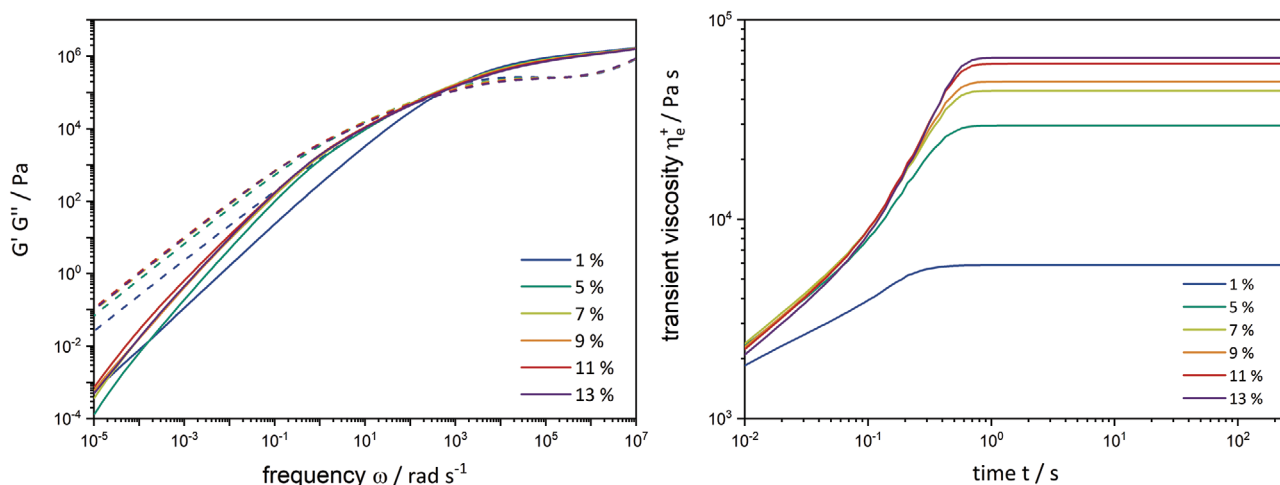
**ADVANCED
SCIENCE NEWS**

www.advancedsciencenews.com

**Macromolecular
Theory and Simulations**

www.mts-journal.de

Figure 7. Microstructural properties of model polymers calculated for a CTA feed stream of 5 mL h^{-1} but for different conversions (3, 6, 9, 12, 15, and 18).
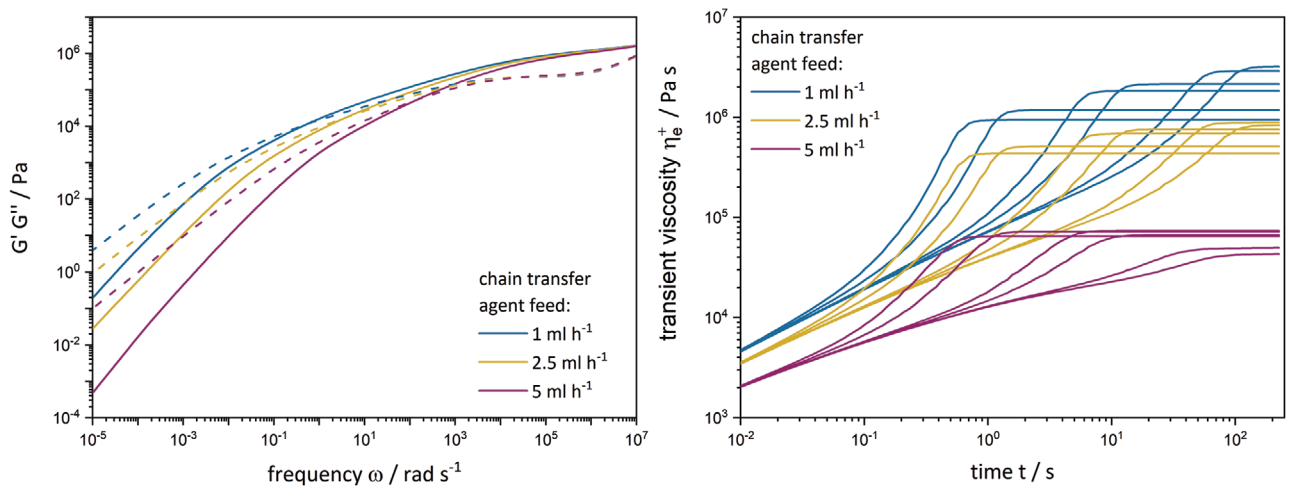
Figure 8. (Left) Linear shear rheology of model polymers calculated for a conversion of 13% but for different CTA feed streams (16, 17, and 18), thus resembling samples with different average molecular weight. Lines represent storage modulus G′, dotted lines the loss modulus G″. (Right) Nonlinear extensional rheology of the same model polymers at strain rates of 10 s^{-1}, 5 s^{-1}, 1 s^{-1}, 0.5 s^{-1}, 0.1 s^{-1}, and 0.05 s^{-1} from left to right.

**ADVANCED
SCIENCE NEWS**

www.advancedsciencenews.com

**Macromolecular
Theory and Simulations**

www.mts-journal.de

Figure 9. Linear shear rheology (left) and nonlinear extensional rheology at strain rate 10 s⁻¹ (right) of model polymers calculated for a CTA feed stream of 5 mL h⁻¹ but for different conversions (3, 6, 9, 12, 15, and 18). For linear rheology lines represent storage modulus G′, dotted lines the loss modulus G″.

interplay of MW, branching frequency, and branching structure for a randomly branched polyethylene. This helps not only to understand and evaluate the partly contrary effects, but also to quantify them on various levels of detail and get a better understanding of how they contribute to the final (mechanical) product properties.

3.2. Evaluating Model and Experiments

After the successful conduction of the sensitivity study, the respective experiments were performed in the lab in order to investigate the effect of chain length and conversion on polymer characteristics experimentally and additionally, test predictability, and model boundaries of the multiscale modeling approach with a wide range of reaction conditions. A detailed list of applied reaction conditions is given in **Table 4**. High-pressure polymerization experiments were performed following the procedure given in the Experimental Section. From an experimental point of view, two factors are noteworthy. 1) Polymerizing ethylene under supercritical conditions leads to reactor fouling. Due to a comparably cooler reactor wall, a polymer-rich boundary layer can be build up there, which reduces heat transfer capabilities and gives rise to very high MW material. This fouling material has a huge impact on polymer properties, especially rheology, due to its high molar mass combined with complex branching. In order to avoid fouling during all performed experiments several precautions were made: the ethylene feed line of the reactor was preheated and not more than five samples were taken per experimental day. Between experimental days, the whole reactor and stirrer were demounted and cleaned thoroughly. 2) Modeling experiments at the same temperature but with different conversions is easily done by adjusting initiator flow. From an experimental point of view, the situation is more complex due to the interplay of external heating, initiator feed, and heat of polymerization, which is of course dependent on absolute conversion. Only by

carefully adjusting both the external heating jacket and initiator feed and reaching steady-state conditions within a reasonable time frame, experiments at the same temperature but with different conversions can be performed successfully.

The LDPE samples obtained by these experiments were characterized by means of triple detector SEC and shear as well as extensional rheology. Average polymer properties of the samples are given in **Table 5**. Number- and weight-average MWs prove that samples with systematically varying chain lengths were produced at varying conversions. Additionally, dispersities increase with increasing conversions as expected from the previously performed modeling study.

Table 4. Summarized reaction conditions for the experiments performed in miniplant: ethene mass flow was always kept at 0.556 g s⁻¹, the residence time at 90 s, and pressure at 2000 bar. Experiments of samples shown here were conducted on five different experimental days, which is indicated by the first number of the labeling. The second number indicates the sample number of the respective experimental day.

experiment	T [°C]	$\dot{m}_{CTA}$ [g s⁻¹]	$\dot{m}_{TBPA}$ [g s⁻¹]	Conversion [%]	f
PA-03–1	245	10.1×10^{-4}	4.17×10^{-6}	13.9	0.428
PA-03–2	245	6.8×10^{-4}	4.17×10^{-6}	13.2	0.389
PA-03–3	245	6.8×10^{-4}	4.17×10^{-6}	13.2	0.389
PA-03–4	240	3.4×10^{-4}	4.17×10^{-6}	12.5	0.371
PA-04–2	250	8.1×10^{-4}	2.50×10^{-6}	7.9	0.244
PA-04–3	250	5.4×10^{-4}	2.50×10^{-6}	9.7	0.349
PA-04–4	250	2.7×10^{-4}	2.50×10^{-6}	8.9	0.292
PA-05–1	248	8.1×10^{-4}	0.00×10^{-6}	0.7	0.040
PA-06–1	245	5.4×10^{-4}	0.00×10^{-6}	0.6	0.036
PA-06–3	245	8.1×10^{-4}	1.96×10^{-6}	6.2	0.215
PA-06–4	250	5.4×10^{-4}	1.96×10^{-6}	6.5	0.220
PA-06–5	245	2.7×10^{-4}	1.96×10^{-6}	6.2	0.215
PA-07–1	245	2.7×10^{-4}	0.00×10^{-6}	1.4	0.080

Table 5. Average polymer properties of miniplant LDPE samples: number-average molecular weight M_n, weight-average molecular weight M_w, and dispersity Đ.

| experiment	M_n [g mol^{-1}]	M_w [g mol^{-1}]	Đ
PA-03–1	17 900	142 900	7.97
PA-03–2	22 200	206 100	9.30
PA-03–3	22 100	215 700	9.76
PA-03–4	27 200	318 200	11.69
PA-04–2	18 500	113 500	6.12
PA-04–3	22 800	168 900	7.40
PA-04–4	28 800	255 800	8.90
PA-05–1	18 900	53 800	2.84
PA-06–1	23 600	71 300	3.03
PA-06–3	18 900	129 900	6.86
PA-06–4	21 400	180 500	8.44
PA-06–5	27 600	239 800	8.68
PA-07–1	39 000	233 500	5.99

In order to directly compare the experimental results with simulations, the simulations from section A were slightly adjusted to resemble the actual reaction conditions during polymerization as given in Table 4. Experimental flow rates and actual temperatures were implemented and initiator efficiency was adjusted within a physically reasonable range ($f = 0.22–0.43$) to meet experimental conversions. This procedure is considered acceptable due to the fact that initiator efficiency depends on reaction conditions and radical surrounding, which is not precisely known under process conditions.
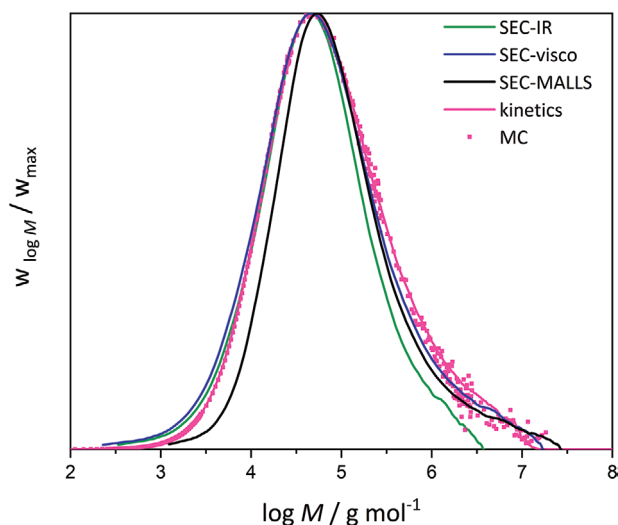
In **Figure 10** MW distributions are given as determined by SEC-IR (dashed lines), kinetic modeling (lines), and Monte Carlo (dots). On the left samples 03–1, 03–3, and 03–4 are

shown, which resemble reaction conditions of 13% conversion, but reduced CTA feed stream. The systematically decreased CTA feed results in an increased MW and broadened MW distribution as expected from the modeling section. Overall agreement of experiments and modeling results is good. Only in the high-MW area deviations are observed, which can be attributed to the insensitivity of the IR detector in the high molar mass low-concentration area rather than to a mismatch of the model, which is shown for the different detector signals in **Figure 11**. In Figure 11 modeling results for sample 03–1 are shown together with SEC-IR, SEC-Visco as well as SEC-MALLS results. Due to the different measurement techniques and thus sensitivities of the detectors, significant deviations between the three detectors are observed. The comparison with the modeling result demonstrates that the modeling fits nicely to the experimental results from the visco and IR detector in the low- and medium-MW area. In the medium- and high-MW area, the modeling results are represented well by the MALLS and visco detector. For better clarity, only the IR detector signal is shown for the other samples. On the right side of Figure 10 MWDs of samples 05–1, 06–3, 04–2, and 03–1 are shown and demonstrate clearly that the experimentally challenging production of LDPE samples with varying conversions, but nearly constant MWs, was successful. With increasing conversion, the MW distributions are significantly broadened, which is clearly visible for both experiments and simulations.

Individual chain behavior in solution is evaluated via the branching ratios, which are given in **Figure 12** for smoothed modeled results (lines) and experimental light scattering (dots). Materials 03–1, 03–3, and 03–4, which resemble LDPEs produced at 13% conversion but with different average chain lengths, are given on the left. For both modeled and experimental results, a reduced average molar mass results in reduced branching ratios due to increased branching. This observation was predicted already by the sensitivity study and can be explained by higher macromolecule concentrations for reduced number-average MW, but identical conversion. However,
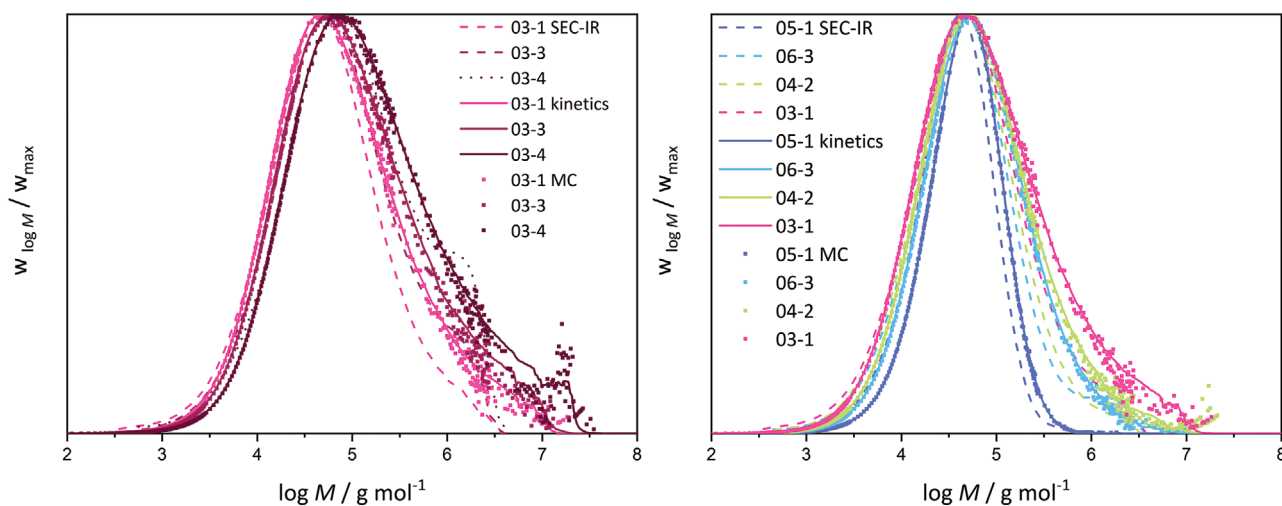
Figure 10. Deterministically (lines), stochastically (dots), and analytically (dashed lines) determined molecular weight distributions for a conversion of X = 13% and varying molecular weights (left) and varying conversions from X = 1–13% but similar molecular weights (right), thus resembling samples with different average molecular weight.

**ADVANCED
SCIENCE NEWS**
www.advancedsciencenews.com

**Macromolecular
Theory and Simulations**
www.mts-journal.de

Figure 11. Molecular weight distributions for 03–1 as modeled deterministically (pink lines) and stochastically (pink dots) as well as measured by SEC-IR (green), SEC-visco (blue), and SEC-MALLS (black).

absolute values of modeled and experimental branching ratios deviate, which was already observed previously.[4] Reasons for this can be found on the experimental side, namely insensitivity of the light-scattering technique at a low molar mass, diffusional broadening during SEC, and the separation according to hydrodynamic volume, which is not strictly proportional to MW. But they also appear in modeling as an ideal random walk is applied for the calculation of radii of gyration.

Branching ratios for samples 05–1, 06–3, 04–2, and 03-1 are given on the right. From a modeling point of view, a reduced branching ratio with increased conversion and thus increased branching is expected. Interpretation of the respective light-scattering results is challenging, due to a strong scatter especially for low conversion sample 05–1 and intersecting

branching ratios. This might be because not identical, but only similar MWs, were reached for the samples. MALLS is strongly sensitive to MW, but not as sensitive toward branching, which could be seen in the sensitivity as well as in Figure 12 (left). Consequently, the not systematical alignment of branching ratios for these samples is probably caused by an overwhelming effect of MW. This demonstrates that also experimentally determined branching ratios should be interpreted with care when it comes to the quantification of long-chain branching. And if validation of branching is to be performed only based on a branching ratio, a model refinement taking into account solvent effects as well as the effect of branching on hydrodynamic volume should be the next step.

Finally, the samples were characterized by means of shear and extensional rheology to assess melt flow behavior. Shear rheology was measured in the linear viscoelastic regime in a parallel plate rheometer for temperatures of 150, 170, and 190 °C. Subsequently, master curves were calculated by performing the Arrhenius shift to 150 °C to access a wider frequency range. Corresponding calculations were done via *SampleBoB* and the BoB algorithm as described in detail in the literature.[4] For all calculations the rheological parameters were used as introduced in the literature (compare **Table 6**).[4,15]

Experimental and modeled linear shear rheology of samples 03–1, 03–3, and 03–2 is given in **Figure 13**. For an increase of MW an increase of both storage and loss modulus is observed and the cross-over point is shifted to lower frequencies. This corresponds to increased viscosities and a more plastic behavior, which is in accordance with expectations and modeling predictions as made in the sensitivity study. When comparing BoB results and experiments, the accordance over the complete frequency range is very high.

Also for samples with similar average MW but different conversions (05–1, 06–3, 04–2, and 03–1), the modeled moduli resemble the experimentally determined ones extremely well. LDPE samples at conversions of 5%, 9%, and 13% exhibit very similar rheological behavior, which was correctly predicted by
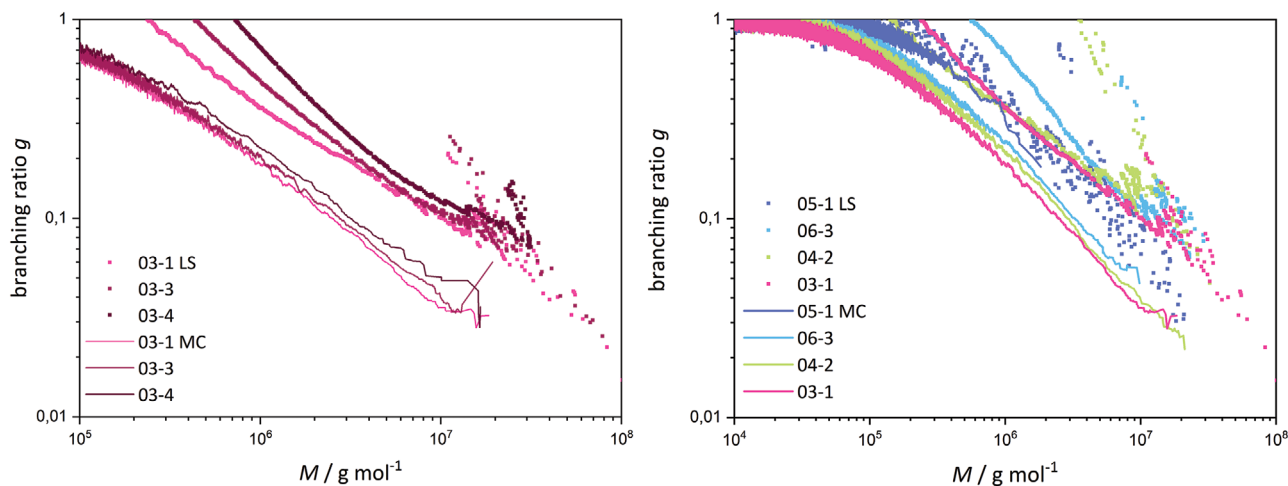
Figure 12. Stochastically (lines) and analytically (dots) determined branching ratios for a conversion of X = 13% but varying CTA feed streams, thus resembling samples with different average molecular weight (left; 03–1, 03–3, 03–4). Branching ratios for samples with similar number-average molar mass but produced at varying conversions (right; 05–1, 06–3, 04–2, 03–1).

Table 6. Rheological input parameters for rheology modeling via branch on branch.

|	
monomer molar mass [g mol^{-1}]	28
density [g cm^{-3}]	0.93
entanglement time τ_e [s]	5.8×10^{-8}
monomers per entanglement N_e	57

the sensitivity analysis. The LDPE sample at 1% conversion shows reduced moduli and cross-over point, which is shifted toward a higher frequency, indicating a lower viscosity due to strongly reduced branching in this sample. This allows two very positive conclusions: 1) Linear rheology is predominantly sensitive toward MW and only slightly sensitive when it comes to long-chain branching. Consequently, only big differences in LCB density (as present for sample 05–1 at 1% conversion) will result in visible effects when examining linear shear rheology. Moreover, it will only be possible to assign them to LCBs rather than MW for certain, if samples of the same molar mass and with different branching levels are investigated. 2) The excellent agreement of modeled and measured data over such a broad region of LDPE properties—with respect to both MW and branching—is a comprehensive validation of the three-step multiscale modeling strategy. The consistency of results proves that the model captures the reaction mechanism—including formation of LCBs—and the underlying kinetics, which are well studied for the investigated system, correctly. At this point, it has to be highlighted again that the presented modeling results were achieved by applying the same data set—from kinetics up to rheological input parameters—so that no parameter fitting was performed in any stage. This proves that the applied modeling approach has a very high predictability, which makes it highly attractive for further and future

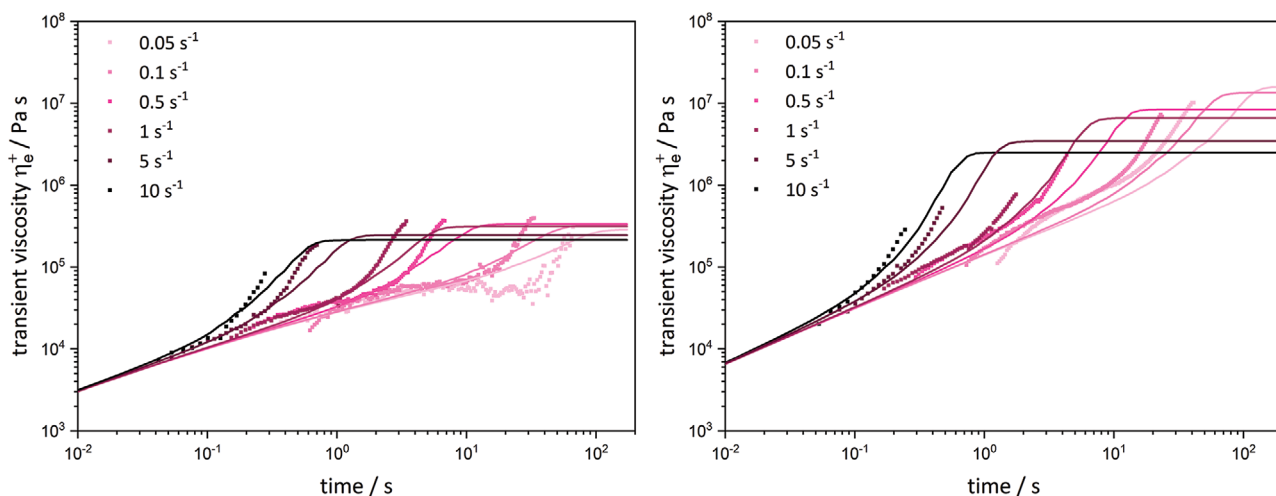investigations in the field of process optimization and product design.

LDPE samples were also characterized by means of extensional rheology over a wide range of strain rates, which is shown exemplarily for samples 03–1 and 03–4 in **Figure 14**. Both samples exhibit pronounced strain hardening for all strain rates, which is demonstrating again the presence of LCBs. Dots represent experiments, while lines are nonlinear rheology modeling results, which were calculated based on the pom-pom equations using only linear rheology as input. Overall agreement of modeled and measured data is very good: onset, slope as well as strain hardening level are estimated satisfactorily by the model. For the low molar mass sample 03–1 lower levels of strain hardening is observed by both model and measurement. It can be traced back to a less complex branching structure exhibiting lower priority values, which was already seen in the sensitivity analysis in Figure 8. This expectation from the modeling side could be proved not only qualitatively, but also semiquantitatively by the performed experiments.

Accordingly, nonlinear extensional rheology could be successfully used to assess flow behavior and processing properties from both the experimental and modeling view. This allowed further model validation and at the same time the understanding of the complex interplay of reaction conditions, random branching and processing properties could be greatly enhanced.

The comparison of experimental and modeled MWDs is always the first step when validating polymerization models with respect to polymer microstructure. However, especially when assessing long-chain branching additional characterization techniques have to be considered. While measuring the branching ratio for LDPE via MALLS gives further insight into the branching structure, the investigation of rheology showed to give an additional valuable model validation in this context.
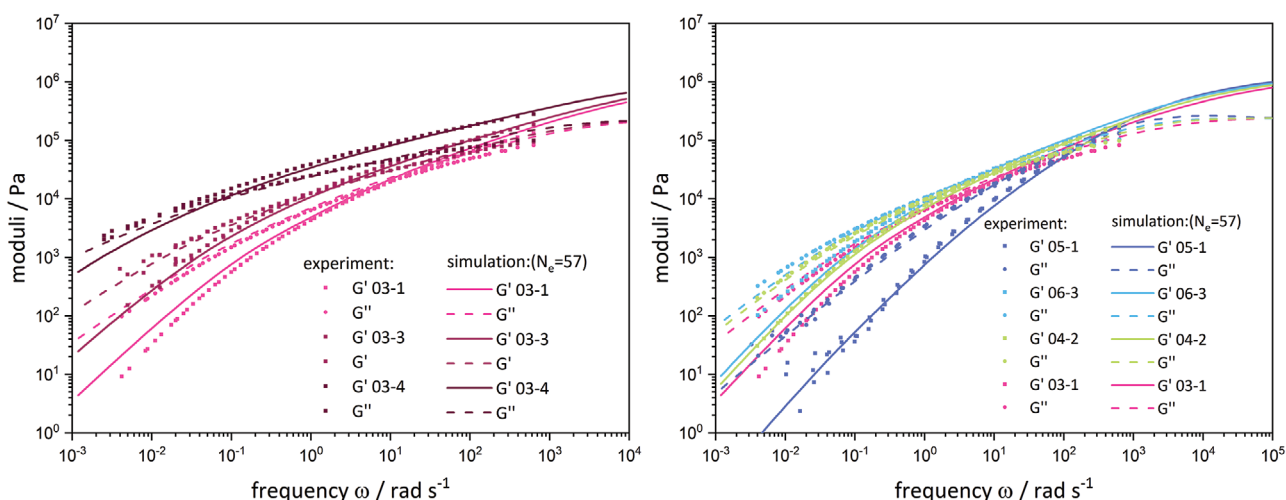
Figure 13. Modeled (lines) and experimentally determined (dots) linear viscoelasticity for a conversion of X = 13% but varying CTA feed streams, thus resembling samples with different average molecular weight (left; 03–1, 03–3, 03–4). Linear viscoelasticity for samples with similar number-average molar mass, but produced at varying conversions (right; 05–1, 06–3, 04–2, 03–1). Storage and loss modulus are shown over a wide frequency range at a reference temperature of 150 °C.

**ADVANCED
SCIENCE NEWS**
www.advancedsciencenews.com

**Macromolecular
Theory and Simulations**
www.mts-journal.de

Figure 14. Modeled (lines) and experimentally determined (dots) nonlinear extensional rheology of samples 03–1 (left) and 03–4 (right) for strain rates from 0.05 s⁻¹ to 10 s⁻¹.

4. Conclusion

Within this work, a newly setup multiscale modeling strategy was applied in a sensitivity study to evaluate the impact of systematically varied reaction conditions on polymeric microstructure and finally rheological properties for LDPE. As the rheology is predominantly determined by MW and degree of long-chain branching, these two parameters were systematically studied by simulating reactions with different CTA concentrations and different conversions. The sensitivity study demonstrated that increased conversions lead to broader MW distributions, increased branching degrees, and branching complexity and consequently also to higher viscosities and increased strain hardening in extension. An increase of CTA concentration on the other hand results in reduced average MW, but increased branching frequency. At the same time, branching complexity—as measured in terms of priority—is reduced. Due to reduced MW and reduced branching depth, viscosities and strain hardening behavior are also predicted to decrease significantly.

In order to check the accuracy of this complex multiscale model, an extensive set of high-pressure miniplant polymerization experiments were performed in accordance with the previously performed study. Respective LDPE samples were characterized by means of SEC, light scattering, and shear as well as extensional rheology. Branching ratio g proved to be a rather insensitive measure for quantifying long-chain branching densities in LDPEs both from an experimental and a modeling perspective. Results were compared to model predictions and very good agreement was observed for polymers prepared under very diverse reaction conditions. These are very encouraging results: 1) They provide further model validation over a very wide and partly unusual range of reaction conditions. 2) They indicate that the complex formation of randomly long-chain branched LDPE is captured correctly by the kinetic model, because otherwise the excellent agreement of modeled and measured rheological behavior for such different samples could not be observed.

The three-step modeling strategy, which is based on basic physicochemical concepts and original models of other works, makes it finally possible to capture the whole picture from process and kinetics to molecular structure and ultimately rheological bulk properties in the linear as well as nonlinear flow regime. It was successfully applied to a broad set of samples LDPE without any parameter adjustments giving good model validation. Further work in this field will focus on the limits of the modeling strategy, optimizations as well as additional applications. Moreover, the modeling approach could be used to enhance the understanding of the complex connection between branching and polymer properties on a molecular level. This also opens up the option of simulation-based process optimizations as well as tailored product designs.

Conflict of Interest

The authors declare no conflict of interest.

[1] J. Asua, *Polymer reaction engineering*, John Wiley & Sons, **2008**.
[2] P. M. Wood-Adams, J. M. Dealy, A. W. deGroot, O. D. Redwine, *Macromolecules* **2000**, *33*, 7489.

**ADVANCED
SCIENCE NEWS**

www.advancedsciencenews.com

**Macromolecular
Theory and Simulations**

www.mts-journal.de

[3] M. Kontopoulou, *Applied Polymer Rheology*, John Wily & Sons Inc. **2011**.

[4] K. M. Pflug, *Linking Reaction Conditions with Polymer Properties for the LDPE Process*, Shaker Verlag **2019**.

[5] M. Busch, *Macromol. Theory Simul.* **2001**, *10*, 262.

[6] a) P. S. E. Bungu, K. Pflug, H. Pasch, *Polym. Chem.* **2018**, *9*, 3142;
b) P. S. E. Bungu, K. Pflug, M. Busch, H. Pasch, *Polym. Chem.* **2018**, *9*, 5051;

[7] C. Gabriel, D. Lilge, *Rheol. Acta.* **2006**, *45*, 995.

[8] a) C. Gabrieland, H. Münstedt, *J. Rheol.* **2003**, *47*, 619;
b) H. Münstedt, D. Auhl, *J. Non-Newtonian Fluid Mech.* **2005**, *128*, 62;

[9] M. Wulkow, *Macromol. React. Eng.* **2008**, *2*, 461.

[10] E. Neuhaus, T. Herrmann, I. Vittorias, D. Lilge, G. Mannebach, A. Gonioukh, M. Busch, *Macromol. Theory Simul.* **2014**, *23*, 415.

[11] D. J. Read, *J. Polym. Sci., Part B: Polym. Phys.* **2015**, *53*, 123.

[12] S. J. O'Donohue, E. Meehan, *ACS Symp. Ser.* **1999**, *731*, 52.

[13] W.-J. Wang, S. Kharchenko, K. Migler, S. Zhu, *Polymer.* **2004**, *45*, 6495.

[14] M. Busch, *Macromol. Theory Simul.* **2001**, *10*, 408.

[15] D. J. Read, D. Auhl, C. Das, J. den Doelder, M. Kapnistos, I. Vittorias, R. C. B. McLeish, *Science* **2011**, *333*, 1871.

[16] a) M. Buback, J. Sandmann, *Z. Phys.Chem.* **2000**, *214*, 583;
b) M. Buback, S. Klingbeil, J. Sandmann, M.-B. Sderra, H. P. Vögele, H. Wackerbatzj, L. Wittkowski, *Z. Phys. Chem.* **1999**, *210*, 61;

[17] M. Buback, C.-R. Choe, E.-U. Franck, *Makromol. Chem.* **1984**, *185*, 1699.

[18] T. Herrmann, *Modellierung technischer Hochdruck-LDPE-Reaktoren*, Uelvesbüll, Der Andere Verlag **2012**.

[19] I. M. Neuhaus, *Modellierung der technischen LDPE Synthese in industriellen Mehrzonenautoklaven*, Uelvesbüll, Der Andere Verlag **2015**.

[20] K. H. Lee, J. P. Marano, *ACS Symp. Ser.* **1979**, *104*, 221.

[21] J. Schweer, *Bestimmung individueller Geschwindigkeitskoeffizienten radikalischer Polymerisationen aus Laserpulsexperimenten mit infrarotspektroskopischer Umsatzdetektion im Mikrosekunden-Bereich*, Dissertation, Georg-August-Universität Göttingen, Germany **1988**.